

Q-Seg: Quantum Annealing-based Unsupervised Image Segmentation

Supreeth Mysore Venkatesh^{1,3}, Antonio Macaluso¹, Marlon Nuske², Matthias Klusch¹, Andreas Dengel^{2,3}

¹German Research Center for Artificial Intelligence (DFKI), Saarbruecken, Germany

²German Research Center for Artificial Intelligence (DFKI), Kaiserslautern, Germany

³University of Kaiserslautern-Landau (RPTU), Kaiserslautern, Germany

{supreeth.mysore, antonio.macaluso, marlon.nuske,
matthias.kluschi, andreas.dengel}@dfki.de

Abstract

In this study, we present *Q-Seg*, a novel unsupervised image segmentation method based on quantum annealing, tailored for existing quantum hardware. We formulate the pixel-wise segmentation problem, which assimilates spectral and spatial information of the image, as a graph-cut optimization task. Our method efficiently leverages the interconnected qubit topology of the D-Wave Advantage device, offering superior scalability over existing quantum approaches and outperforming state-of-the-art classical methods.

Our empirical evaluations on synthetic datasets reveal that *Q-Seg* offers better runtime performance against the classical optimizer Gurobi. Furthermore, we evaluate our method on segmentation of Earth Observation images, an area of application where the amount of labeled data is usually very limited. In this case, *Q-Seg* demonstrates near-optimal results in flood mapping detection with respect to classical supervised state-of-the-art machine learning methods. Also, *Q-Seg* provides enhanced segmentation for forest coverage compared to existing annotated masks. Thus, *Q-Seg* emerges as a viable alternative for real-world applications using available quantum hardware, particularly in scenarios where the lack of labeled data and computational runtime are critical.

1. Introduction

Image segmentation is pivotal in computer vision, enabling pattern recognition across diverse applications including medical imaging [41, 62], autonomous navigation [25, 42], search engines [80], and earth observations [48]. Technically, segmenting an image consists of partitioning it into non-overlapping regions with distinct attributes, aligning with human perception [83]. The continual advancement of algorithms has propelled computer vision research, yielding

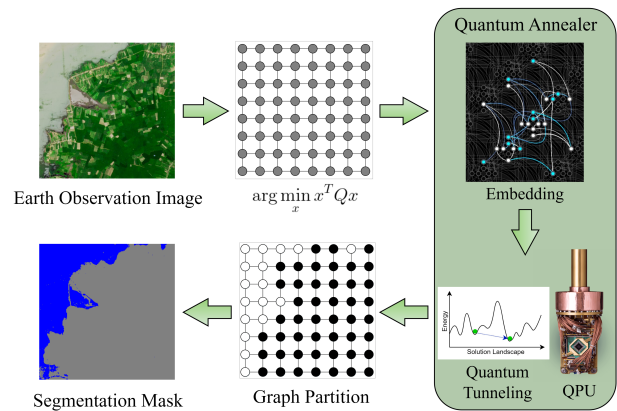


Figure 1. The proposed *Q-Seg* for unsupervised image segmentation generates a graph representing the original image. The distinct semantic regions in the image are identified by finding the minimum cut in the graph, an NP-hard problem that can be formulated as Quadratic Unconstrained Binary Optimization (QUBO). The QUBO problem is subsequently encoded into the physical topology of the D-Wave quantum annealer. Leveraging quantum tunneling, the annealing process efficiently explores an exponentially large solution space to locate the global optimum, which can be decoded as the segmentation mask.

substantial performance enhancements. Nevertheless, algorithm design remains closely linked to the capabilities of the underlying hardware [73].

Recently, quantum computing has emerged as a powerful alternative to solve complex real-world applications [18, 24]. However, current quantum computers have limited capabilities, impacting algorithm design and testing. Specifically for computer vision, several quantum methods have been proposed for image classification [39, 56–58], multi-object tracking [84], image matching [10, 11, 57], motion segmentation [7], edge detection [31, 79, 81, 85] and image segmentation [64, 73]. Nonetheless, all these approaches do not show a concrete advantage for practical

applications using existing quantum hardware.

In this paper, we introduce *Q-Seg*, a novel unsupervised method that formulates the image segmentation problem as a graph-based optimization task, solvable via quantum annealing. The vast solution space, exponential in pixel count, is efficiently navigated to yield near-optimal segmentation congruent with contemporary annealer architectures. To show the ready-to-use capability of our approach, we run experiments using the *D-Wave Advantage* annealer on synthetic and real-world satellite imagery datasets, specifically for Forest Cover [29] and Flood Mapping [15]. In the case of Forest Cover segmentation, we obtain high-quality masks, underscoring the value of unsupervised methods in scenarios with noisy or uncertain ground truth. For Flood Mapping, we achieve near-optimal segmentation quality, rivaling supervised methods. These results highlight capability of *Q-Seg* to segment small and medium-sized images with existing quantum annealers, benchmarked against the classical state-of-the-art optimizer *Gurobi* for a comprehensive assessment of both runtime and segmentation efficacy.

The paper proceeds with Section 2 discussing related works, followed by preliminaries in Section 3. Our method is presented in Section 4, with experimental evaluations in Section 5, and we conclude in Section 6.

2. Related Works

State-of-the-art methods for image segmentation primarily involve the use of Deep Convolutional Neural Networks in a supervised manner. These approaches can achieve exceptionally precise segmentation performance when supplied with accurate annotations [65]. However, in various domains acquiring labeled data encounters challenges such as the considerable cost and time required for manual annotation, the necessity for domain expertise, and scalability issues when handling large datasets. Also, subjectivity among annotators and variations in interpretation can introduce inconsistencies.

These limitations underscore the importance of unsupervised techniques, especially when leveraging vast unlabeled datasets [4, 77, 78]. Unsupervised segmentation algorithms can be classified into several categories. Thresholding is a pixel-wise segmentation method that assigns pixels to regions based on intensity values [61]. While computationally efficient, it is susceptible to issues arising from illumination variations and noise, which reduce its effectiveness in situations where factors beyond intensity affect performance [67, 71]. On the other hand, feature space clustering segments the spectral feature space into distinct clusters, each representing an image region [54]. However, a notable limitation of this approach is its disregard for spatial relationships between pixels [27, 46, 63]. Edge-based segmentation techniques detect discontinuities in image attributes, primarily pixel intensities, to delineate object boundaries

[13, 26]. While adept at handling images with clear object edges this method struggles with noisy or indistinct boundaries, resulting in segmentation errors. Region-based methods, on the other hand, focus on pixel homogeneity. Techniques like region-growing initialize with seed pixels and expand regions based on similarity metrics until a set condition is satisfied [12, 13, 55, 63]. Conversely, region-splitting dissects larger segments into finer clusters when they lack homogeneity in attributes like color, texture, or intensity [13, 48, 55]. However, region-based methods falter with scenarios where objects exhibit attribute similarities or when similarity thresholds are not optimally set, resulting in over-segmentation or under-segmentation [38, 70].

Graph-based segmentation conceptualizes image segmentation as a graph partitioning task where nodes correspond to pixels or regions, while edges, weighted by pixel dissimilarity, link adjacent nodes [5, 22, 30, 33]. The primary goal is to discern subgraphs that align with coherent clusters in the image. A salient feature of this approach is its capacity to amalgamate both boundary and regional information, yielding globally optimal solutions for specific cases [32, 34]. This makes it a potent tool for image segmentation, especially when prior data is sparse [82]. However, the inherent complexity of optimization tasks, such as graph cuts or clustering, renders the method computationally demanding [9, 28, 76].

Recent research has ventured beyond classical computing paradigms, exploring quantum algorithms for computer vision tasks [49]. For instance, the application of the Inverse Quantum Fourier Transform (QFT) for segmentation [3] has been investigated. However, implementing the QFT requires a fault-tolerant gate-based quantum computer. Quantum circuit-based thresholding for segmentation has been explored [23], though such tasks are already efficiently handled by classical systems [66, 68], emphasizing the need for quantum approaches in more complex scenarios. Graph-based segmentation using variational quantum circuits has been investigated [73]. However, the method has scalability issues in practical applications, as the qubit requirements, corresponding to the number of image pixels, limit their feasibility for large-scale use. Lastly, a hybrid approach is presented in [60], where a quantum annealer facilitates feature extraction, and segmentation is executed classically.

Recently, the use of quantum annealing for image segmentation [64] has been investigated. The concept involves formulating segmentation as a constrained optimization problem, which can be transformed into an unconstrained problem by embedding constraints through penalty terms in the cost function. However, the accurate estimation of penalty parameters significantly impacts the performance of quantum annealing and presents notable scalability challenges on current quantum annealers [8]. This limitation arises from the constrained connectivity among qubits, re-

stricting the applicability of this approach.

3. Preliminaries

In contemporary quantum computing, two distinct paradigms have emerged for tackling diverse problem sets: universal gate quantum computing and adiabatic quantum computing (AQC). This paper zeroes in on the adiabatic quantum computing paradigm, a computational approach that employs the quantum annealing process to address quadratic unconstrained binary optimization (QUBO) problems, defined as follows [35]:

$$\arg \min_x x^T Q x = \arg \min_x \sum_{i=1}^n c_{ii} x_i + \sum_{1 \leq i < j \leq n} x_i (1 - x_j) q_{ij} \quad (1)$$

where $x \in \{0, 1\}^n$ is the binary variable vector and $Q \in \mathbb{R}^{n \times n}$ is the QUBO matrix, with its diagonal and off-diagonal elements representing linear and quadratic coefficients, respectively. Despite its straightforward formulation, solving the QUBO problem is NP-hard [6, 35, 36], presenting significant computational challenges for large-scale instances since the solution space grows exponentially with the input size [43, 50]. This complexity is a hallmark of discrete optimization landscapes where input perturbations can yield non-linear cost deviations, i.e., small changes in input can lead to large variations in the cost function [45].

Quantum annealers, utilizing the principles of quantum mechanics, particularly the adiabatic theorem [17], efficiently navigate complex solution landscapes. Through quantum tunneling, these devices can potentially escape local minima, offering a promising alternative to classical optimization methods [1, 14]. However, the practical implementation of large QUBO problems on quantum annealers is hindered by limitations such as a finite number of qubits, connectivity constraints, susceptibility to noise, and sensitivity to optimization landscape and algorithmic characteristics. Thus, identifying suitable problems is essential for unlocking the full potential of quantum annealing in tackling complex optimization tasks.

4. Methods

This section describes in detail *Q-Seg*, delineating the algorithmic workflow, encapsulating the preprocessing, problem formulation, quantum annealing process, and how to obtain the segmentation mask.

Image to Graph The method initiates by constructing a lattice graph of the input image with a grid-graph topology [2]. In this representation, graph nodes equate to image pixels, preserving the spatial inter-pixel connectivity crucial for segmentation. Instead, the edge weights between

nodes must reflect the extent of the similarity (or dissimilarity) between neighboring pixels. The choice of how to define the edge weights is application-dependent, and different applications may require distinct metrics tailored to specific characteristics of the image data.

When representing an image as a graph, segmentation involves identifying a graph cut that partitions the vertices based on the similarity metric of edge weights. Specifically, when the edge weights represent pixel similarity, dividing the graph into semantically distinct regions can be framed as discovering the minimum cut in the graph, minimizing the sum of cut edges' overall similarity. Conversely, when edge weights measure pixel dissimilarity, the segmentation task targets the maximum cut. Notice that, assuming real-value edge weights, the maximum cut problem can be transformed into a minimum cut problem by negating the edge weights and vice-versa [69]. Consider an undirected weighted graph $G(V, w)$ with no self-loop edges, where V is the set of vertices and $w : V \times V \rightarrow \mathbb{R}$ is the edge weight function. In this context, a 'cut' denotes the partitioning of the graph into disconnected subgraphs, which arises from the removal of a specific set of edges. The *cost* of a cut is quantified as the aggregate of the weights of the edges removed as follows:

$$MINCUT(G) = \arg \min_{A, \bar{A}} \sum_{i \in A, j \in \bar{A}} w(v_i, v_j) \quad (2)$$

$$\text{such that } A \cup \bar{A} = V, A \cap \bar{A} = \emptyset$$

where $w(v_i, v_j)$ is the weight of the edge connecting the nodes v_i and v_j . In its general formulation where edge

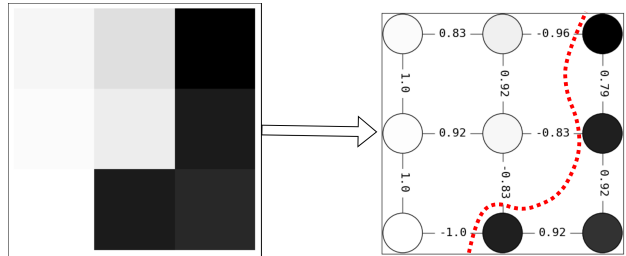


Figure 2. Converting the pixel values into edge weights in the grid graph. The grid structure of the graph captures the spatial information (high-level information such as regions or objects) and the edge weight captures the spectral information (low-level information such as pixel values). The red-colored dotted curve passes through the set of edges that divide the vertices into two distinct sets, such that the sum of the edge weights is minimum.

weights can be positive and negative values, finding the minimum (or maximum) cut in the graph is NP-Hard, and there is no classical solution [37, 44] that can solve the problem efficiently. Indeed, for an image with n pixels, there

exist 2^n potential solutions, rendering exhaustive enumeration of all possible solutions infeasible. Fig. 2 provides an illustration of converting a grey image of size 3×3 to a grid graph where the edge weights $\in [-1, 1]$ represent the similarity between the neighboring pixels.

Formulating QUBO To overcome the computational hurdles on a classical computer, and be able to segment an image efficiently we make use of a quantum annealer. This necessitates recasting the minimum cut problem into QUBO form, which is compatible with the operational framework of quantum annealing. A cut is also conceptualized as the bifurcation of the vertex set into two exclusive subsets, with a minimum cut characterized by the least possible sum of edge weights bridging these subsets. If G has n nodes, associating a binary variable x_{v_i} to vertex v_i for all $i \in \{1, 2, \dots, n\}$ allows to encode the solution as $v_i \in A \forall x_{v_i} = 0$ and $v_i \in \bar{A} \forall x_{v_i} = 1$ or vice-versa. The objective function for computing the minimum cut in this binary framework is articulated as [35, 50]:

$$x^* = \arg \min_x \sum_{1 \leq i < j \leq n} x_{v_i}(1 - x_{v_j})w(v_i, v_j) \quad (3)$$

where $x = x_{v_1}, x_{v_2}, \dots, x_{v_n}$ and $x_{v_i} \in \{0, 1\}$

The cost function in Eq. (3) is equivalent to the formulation of the QUBO problem in Eq. (1) [75]. Given the edge weights $w(v_i, v_j)$, substituting them into Eq. (3) and simplifying yields a quadratic expression in binary variables x_{v_i} where $i \in \{1, 2, \dots, n\}$. The construction of the Q matrix in Eq.(1), is derived from the coefficients of terms in the quadratic equation. Note that the QUBO formulation of the minimum cut does not introduce any computational overhead in terms of the number of variables compared to the input in the original problem, as is the case with other existing formulations [64, 74].

QUBO with Quantum Annealing Quantum annealing offers a probabilistic approach to solving the QUBO problem through the exploitation of quantum tunneling and entanglement. The process begins by mapping the QUBO onto the topology of physical qubits, aligning the solution with the binary states of the qubits. Throughout the annealing process, the system evolves from a superposition of all possible states toward the lowest energy state, corresponding to a state where the optimal QUBO solution has a high probability of being measured. This evolution is governed by the annealing schedule, which carefully balances quantum and classical energies to avoid local minima.

The *D-Wave* quantum annealer, in particular, employs a specialized hardware design conducive to this process, making it well-suited for graph-based problems like image segmentation. Through iterative adjustments of the system’s

parameters and repeated annealing cycles, the probability of discovering the global minimum increases. The final read-out produces a binary string directly translating into the segmented image.

To summarize, the *Q-Seg* approach is described in Fig. 1, and the pseudo-code is shown in Algorithm 1.

Algorithm 1 Outline of *Q-Seg*

Require: Image I with n pixels

Ensure: Segmentation mask M matching I ’s dimensions

- 1: Construct grid graph $G(V, w)$ from image I
 - 2: Formulate QUBO for minimum cut on G (Eq. (3))
 - 3: Map the QUBO to the quantum annealer’s architecture
 - 4: Execute quantum annealing to optimize the QUBO
 - 5: Extract the lowest-energy sample X^*
 - 6: Decode sample X^* into segmentation mask M
-

Pseudocode For an input image I , we construct a grid graph G with a one-to-one correspondence between pixels in I and vertices in G . Edge weights $w(v_i, v_j)$ are assigned based on pixel similarity between v_i and v_j , with the goal of segmenting I by identifying a minimum cut in G . The QUBO formulation captures this objective, translating the problem into a format amenable to quantum annealing. The annealing process is iterated multiple times to ensure the reliability of the solution, which is then decoded into a binary mask M as $M_i = x_{v_i}$ for each vertex $v_i \in V$, describing the segmented regions of I .

The structure of the graph in our problem formulation, with nodes exhibiting a maximum degree of 4, naturally fits the architecture of the existing quantum annealer hardware [52]. This congruence facilitates efficient mapping of logical to physical qubits, reducing the number of cloned qubits and inter-qubit coupling. Consequently, as we will see in Section 5, this enhances the fidelity of the annealing outcomes.

5. Experiments

In this section, we present experimental evaluations of *Q-Seg* against state-of-the-art classical methods on a synthetic dataset and two practical use cases in the domain of earth observation.

5.1. Experimental settings

5.1.1 Datasets

Synthetic Data: The complex operation in *Q-Seg* involves computing the minimum cut in a grid graph, a key step essential for effective image segmentation. We generate synthetic datasets comprising undirected, connected, and weighted grid graphs of square structure, with sizes ranging

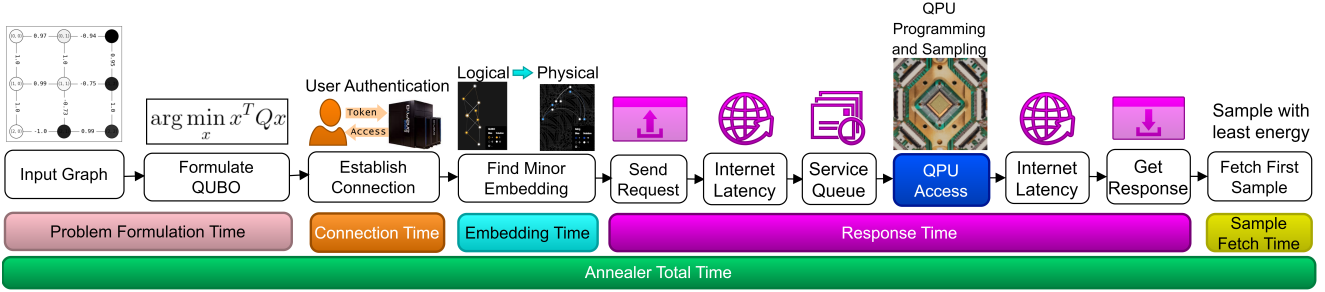


Figure 3. The figure illustrates the operational pipeline of *D-Wave* quantum annealer. It begins with reformulating the minimum cut problem as a QUBO, followed by authentication using a private token for remote access. The *minorminer* [20] tool maps the logical qubits in QUBO to the physical qubits in hardware. The problem instance is sent over the internet to join the queue on the shared *D-Wave* device. The Quantum Processing Unit (QPU) performs the annealing process, producing a set of samples. The final step is extracting the optimal solution, identified by its lowest energy state that encodes the segmentation mask.

from 2×2 up to 44×44 . This data allows assessing the performance of *Q-Seg* in terms of runtime while increasing the problem size. For reproducibility, we employ a fixed seed to assign edge weights, which are randomly selected from a uniform distribution within the interval $[-1, 1]$ ensuring that the edge weights to be both, positive and negative. Tests are conducted on five sets of graphs, each initialized with a different seed.

Forest Cover: Forest segmentation is crucial for ecological sustainability enabling accurate assessment of deforestation rates, forest density, and changes due to climatic or human factors. Due to the limited availability of time resources of the real quantum device, we randomly sample a subset of images from the *DeepGlobe18* dataset [29], each measuring 256×256 pixels, accompanied by binary segmentation mask. Furthermore, the original images are downsampled to 32×32 pixels, to fit the actual number of qubits in the real device. In particular, the preprocessing steps included median blurring and conversion to the HSV (Hue Saturation Value) color scale [72], tailored to the requirements of the specific use case. For generating the input graph for *Q-Seg* algorithm, we incorporate the Gaussian similarity [59] as the edge weight metric, normalizing them within the range of $[-1, 1]$.

Flood Mapping: The *Sen1Floods11* dataset [15], designed for water segmentation in satellite imagery, comprises georeferenced samples with dimensions of 512×512 pixels across 13 spectral bands. The ground truth masks include binary labels and an additional value of -1 , indicating uncertain areas, as annotated by experts. Specifically, the subset of images used comprises pictures of the Bolivia region obtained from [40]. The images are segmented at a pixel level, and then we work with 32×32 patches and subsequently integrate these patches to form the complete segmentation mask. This approach allowed for detailed analysis without compromising image integrity.

For generating the graph, we first calculated the normal-

ized difference water index [21, 51] of the input images and used a normalized Gaussian similarity metric [59] for edge weights. The quality of this segmentation is evaluated against metrics outlined in Section 5.1.3.

5.1.2 Solving methods

Our experiments were conducted using the *D-Wave Advantage* quantum annealer for the graph-cut optimization, accessed through a cloud service via the *dimod*¹ library. This device comprises 5670 physical qubits and has a *pegasus* topology [16, 52, 53]. For benchmarking against classical approaches, we implemented the *Gurobi* v9.5.2 optimizer to solve the QUBO problem representing the minimum cut. Furthermore, to calculate the typical metrics used for segmentation (*IoU*, *Accuracy*, *Precision*, *Recall*), we compare the results of *Q-Seg* for the Flood Mapping dataset with a state-of-the-art supervised method that uses gradient-boosted decision trees (GBDT) [40]. The classical part of our experiments was conducted on a system equipped with an *Intel(R) Xeon(R) CPU @ 2.20GHz* and *8 GB* RAM, with all software developed in *Python 3.9*.

5.1.3 Metrics

We evaluate our method using three different types of metrics: *runtime*, *quality* and *scalability*.

The *runtime* allows us to estimate the efficiency of *Q-Seg* in comparison to classical state-of-the-art optimizers. In Fig. 3, a comprehensive description of all components of the quantum annealing pipeline is presented, emphasizing their significance when executing a problem on a real quantum device in the cloud.

In terms of *quality*, we evaluate *Q-Seg* using a set of established metrics. These include *Intersection over Union*

¹https://docs.ocean.dwavesys.com/en/stable/docs_dimod/

(IoU) to assess the accuracy of overlap in segmented regions, *Accuracy* for determining the correct segmentation of pixels, *Recall*, and *Precision* to evaluate the detection and accuracy of segmentation boundaries.

Additionally, to assess the segmentation carried out by *Q-Seg* in comparison to deterministic methods, we conducted a comparison of minimum cut values, employing the relative error as the metric for evaluation, defined as [19]:

$$E_r = \left| \frac{V_G - V_{QA}}{V_G} \right| \quad (4)$$

where V_G represents the minimum cut value from *Gurobi* and V_{QA} from the *D-Wave Advantage* annealer.

Finally, we assess the *scalability* of *Q-Seg* by quantifying *Qubit Complexity*, i.e., the number of physical qubits required in a real quantum device with respect to other existing quantum-annealing-based approaches.

5.2. Results

5.2.1 Runtime Analysis

We ran *Q-Seg* on the synthetic dataset using both the *D-Wave Advantage* and *Gurobi* to compare classical and quantum algorithms while progressively increasing the problem size. The results, which encompass all the distinct components in the entire quantum annealing pipeline (Fig. 3), are illustrated in Fig. 4. We observe that even when factoring in the runtime, which includes the response time from sending the problem to receiving the solution from the *D-Wave* annealer—involving internet latency, queuing due to shared annealer usage, and the annealing process—the total time-to-solution for quantum annealing is significantly lower than that of *Gurobi* that executes locally.

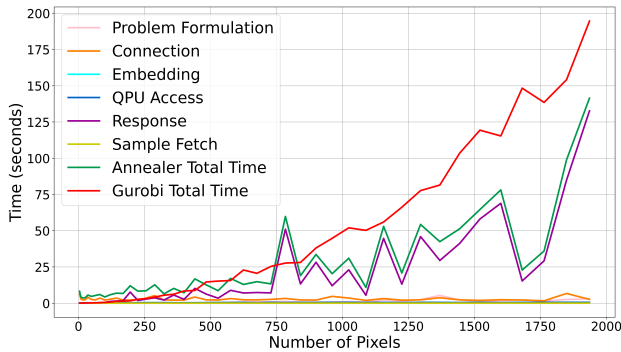


Figure 4. Runtime comparison between *D-Wave Advantage* annealer and *Gurobi* for the synthetic data with $seed = 333$. This graph illustrates the breakdown of annealer runtime, highlighting the components in Fig. 3. Despite shared and remote access, the *D-Wave Advantage* demonstrates a consistently shorter total runtime compared to *Gurobi*'s local execution.

In a hypothetical scenario with a dedicated QPU, we could omit the connection establishment, internet latency,

and queuing, which are significant contributors to the total runtime. This assumption allows for a more direct comparison of the annealer's efficiency against *Gurobi*. In particular, *QPU Access Time* reflects the Quantum Processing Unit's active problem-solving duration. This metric can be divided into *QPU Programming Time*, *QPU Sampling Time*, and *QPU Access Overhead Time*. The programming phase sets up the QUBO model in the annealer, sampling involves the actual annealing process, and the overhead time is associated with post-processing the samples.

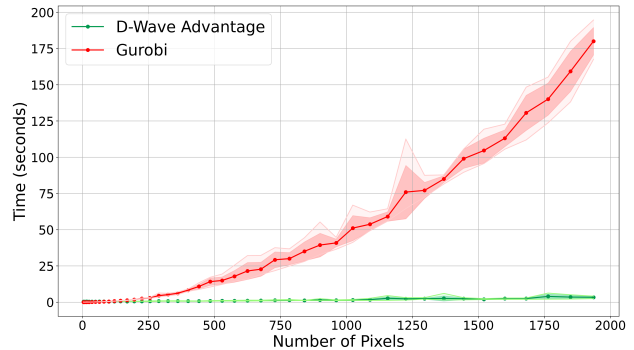


Figure 5. The plot illustrates the mean runtime (represented by a solid line), the range of runtimes (indicated by the broadly shaded area), and the standard deviation (denoted by the lightly shaded area) is aggregated over five sets of synthetic data for the minimum cut operation on graphs of square images of varying sizes. The results highlight the efficiency of *Q-Seg*, especially evident in processing larger images.

Fig. 5 compares the runtime of *D-Wave Advantage* and *Gurobi* assuming a dedicated onsite QPU. The hybrid process, involving QUBO formulation, embedding, annealing, and solution retrieval, exhibits even more pronounced superior performance compared to the previous scenario, especially as the problem size increases. This efficiency can be attributed to the grid graph structure aligning well with the QPU architecture. The newer *D-Wave* devices, featuring enhanced qubit connectivity, further enhance this efficiency, making *Q-Seg* particularly effective on these platforms [47].

5.2.2 Quality

While *D-Wave* exhibits faster processing than *Gurobi*, it is essential to evaluate the quality of the solutions. The analysis depicted in Fig. 6 shows that although *Gurobi* consistently produces slightly superior solutions, the margin is minimal. This observation is further supported by the relative error trends across different problem sizes. Thus, our approach showcased the ability to address large-scale problems with commendable quality using current quantum hardware. With an onsite annealer, the limitations on the number of annealing cycles, impacting the quality of so-

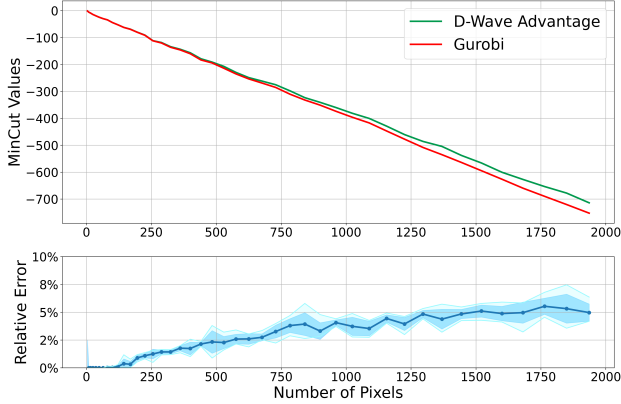


Figure 6. The first plot contrasts the minimum cut values obtained by *Gurobi* and the *D-Wave Advantage* annealer on synthetic data with $seed = 333$, highlighting *Gurobi*'s marginally better performance. The trend of diminishing values substantiates the rising count of negative edges that are cut as the problem size increases. To substantiate a consistent behavior, the second plot shows the mean (represented by the solid line), range (depicted by the broadly shaded area) and standard deviation (illustrated by the narrow shaded area) of the relative errors in the annealer solutions compared to *Gurobi* across five sets of the synthetic data.

lutions, could be mitigated, potentially elevating solution quality.

Forest Cover Segmenting Forest Cover poses a significant challenge, primarily attributed to the presence of noisy and inconsistent ground truth labels in the dataset. This inconsistency can introduce bias during the training of supervised methods, potentially leading to misleading comparisons between algorithmic outcomes and dataset ground truth masks. Fig. 7 provides a qualitative glimpse into the segmentation results of *Q-Seg* against existing masks.

A visual examination of the segmentation masks produced by *Q-Seg* underscores the need for robust unsupervised segmentation methods in situations where supervised methods struggle with noisy labels and irregularities. Our approach showcases its potential to provide more reliable and visually consistent segmentation results in such challenging environments. Importantly, the consistency of poor-quality ground truth and the corresponding high-quality masks provided by *Q-Seg* is uniform across all the images in the available dataset.

Flood Mapping Commonly, state-of-the-art methods for image segmentation rely on supervised learning, utilizing annotated masks to train algorithms for correctly identifying masks in unannotated images. In the context of the Flood mapping dataset, the GBDT stands out as the state-of-the-art method, even outperforming CNNs in this specific

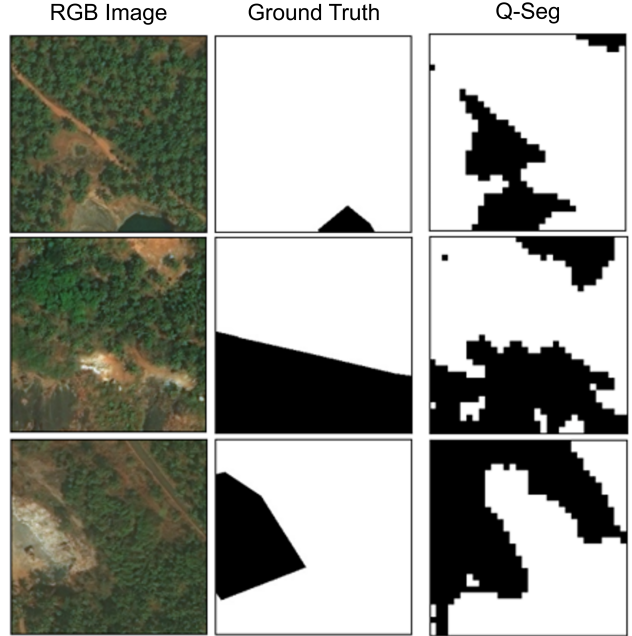


Figure 7. Visualization of RGB images, ground truth masks, and *Q-Seg* segmentation results in the Forest Cover use case. The ground truth masks show noisy labeling and irregularities, while the *Q-Seg* results reveal more coherent and visually refined segmentation of Forest Cover.

case [40]. To evaluate the performance of *Q-Seg* in terms of quality of the segmentation, we compare the results with the GBDT. Results are shown in Table 8.

As expected, the supervised approach outperforms *Q-Seg* in the majority of metrics, except for *Precision* where *Q-Seg* exhibits better performance. Nevertheless, *Q-Seg* delivers commendable results, closely trailing the supervised approach despite being an unsupervised method. This underscores the efficacy of *Q-Seg* in providing high-quality segmentation results without the need for extensive training or reliance on expertly annotated data.

Metrics	GBDT [40]	<i>Q-Seg</i>
IoU	0.888	0.775
Accuracy	0.913	0.828
Recall	0.993	0.780
Precision	0.892	0.990
F1-score	0.935	0.861

Table 1. Performance Comparison of the supervised approach GBDT [40] against *Q-Seg* in Flood Mapping use case. The metrics are evaluated ignoring the unsure pixels in the ground truth.

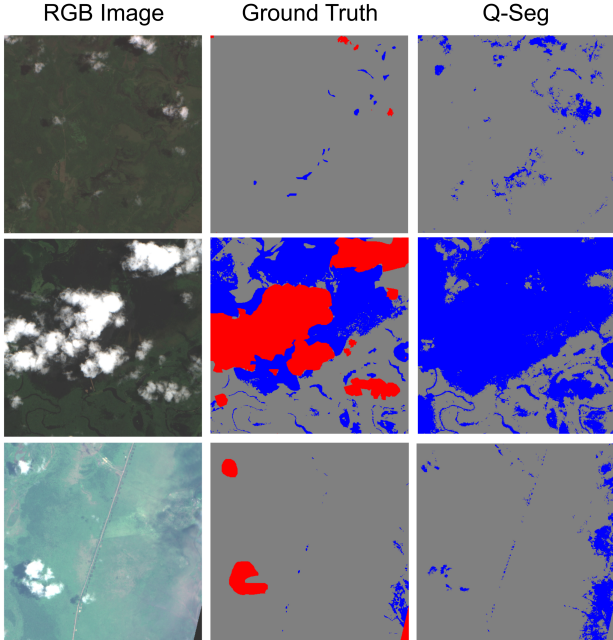


Figure 8. Visualization of RGB images, expert-labeled ground truth masks, and Q -Seg segmentation results in Flood Mapping. The segmentation differentiates water (blue), dry land (grey), and uncertain areas (red) affected by cloud coverage.

5.2.3 Scalability

In this section, we delve into the scalability of our method, particularly in the context of current quantum annealing technologies and their near-term advancements. Our focus is on assessing the adaptability of Q -Seg to the evolving landscape of quantum computing, especially in comparison to another quantum annealer-based image segmentation method used for Synthetic Aperture Radar (SAR) images [64]. A critical aspect of our analysis is the compatibility of Q -Seg with the topological structure of the D -Wave Advantage quantum annealers. Unlike the approach in [64], Q -Seg demonstrates a better utilization of the quantum hardware capabilities by efficient embedding of logical qubits in the QUBO matrix to the physical qubits of the annealer.

Our empirical results, as shown in Fig. 9, reveal a substantial reduction in the physical qubits required for Q -Seg compared to the method in [64]. This efficiency arises from Q -Seg’s problem formulation: for an image with n pixels, it necessitates n vertices, each with a maximum rank of 4. In contrast, the approach in [64] utilizes $n + 2$ vertices, with the additional vertices having a rank of n . The edges in the graph represent logical qubit interactions, where assigning a logical qubit with extensive interactions to a physical qubit in the QPU poses challenges, requiring multiple physical qubit clones for effective representation. This directly impacts the annealer’s performance, as an ideal embedding

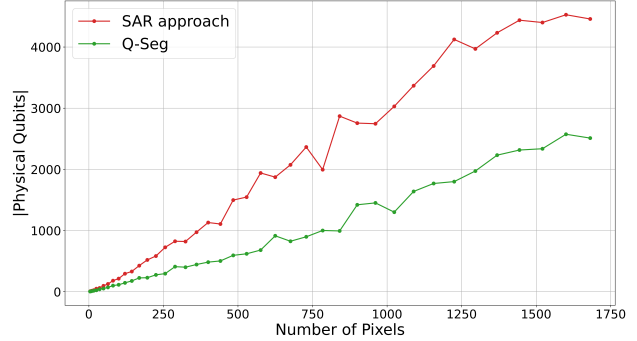


Figure 9. Comparison of physical qubit needs for Q -Seg and SAR segmentation [64] on the D -Wave Advantage with varying image sizes. The qubit requirements are estimated using the *minorminer* [20] tool given the logical qubit interactions in the QUBO problem and the available couplers in the annealer hardware.

involves a one-to-one mapping of logical to physical qubits. Furthermore, the solution space complexity in [64] is 2^{n+2} , four times that of Q -Seg. Given that there are only up to 2^n possible binary segmentations of the image, all encompassed within Q -Seg’s solution space, it suggests a prevalence of redundant solutions in the method of [64].

6. Conclusion

In this paper, we introduced Q -Seg, a novel unsupervised segmentation algorithm designed specifically for existing quantum annealers. By efficiently reformulating the segmentation task as a minimum-cut problem in a graph and subsequently as a QUBO problem, our proposed quantum approach efficiently leverages the hardware topology of D -Wave annealers, harnessing the advantages of quantum computing. This not only enhances scalability but also ensures the generation of high-quality solutions using near-term quantum devices.

Our experiments on synthetic data with simulated images of increasing sizes demonstrate a significant runtime advantage of Q -Seg in processing large-scale images compared to the state-of-the-art optimizer *Gurobi* (Fig. 4, 5). Notably, this runtime advantage is achieved without a significant impact on the quality of segmentation (Fig. 6).

To validate our approach on real-world data, we applied Q -Seg to two different earth observation tasks: Forest Cover and Flood Mapping. The Forest Cover dataset experiments reveal that Q -Seg can generate superior masks compared to the available ground truths (Fig. 7), showcasing its potential in scenarios with limited or unreliable labeled data. This performance highlights the significant impact of quantum computing in its current state to enhance image segmentation.

Additionally, for the Flood Mapping use case, we conducted a comparison between the masks generated by Q -

Seg and a classical supervised approach (GBDT) (Fig. 8). Despite the results of *Q-Seg* being suboptimal in terms of *IoU*, *Accuracy*, *Recall*, and *F1-score*, it demonstrated superior *Precision* compared to the supervised approach (Table 1). This noteworthy outcome is particularly significant as *Q-Seg* achieved higher *Precision* without relying on annotated masks. In conclusion, this study establishes the foundation for future progress in quantum-enhanced computer vision, pointing towards a promising path for tackling progressively complex problems with existing quantum technology.

Code Availability

All code to generate the data, figures, analyses, as well as, additional technical details on the experiments are publicly available at <https://github.com/supreethmv/Q-Seg>.

Acknowledgments

This work has been partially funded by the German Ministry for Education and Research (BMB+F) in the project QAI2-QAICO under grant 13N15586.

References

- [1] Steve Abel, Andrew Blance, and Michael Spannowsky. Quantum optimization of complex systems with a quantum annealer. *Phys. Rev. A*, 106:042607, 2022. 3
- [2] BD Acharya and MK Gill. On the index of gracefulness of a graph and the gracefulness of two-dimensional square lattice graphs. *Indian J. Math*, 23(81-94):14, 1981. 3
- [3] Taoreed Akinola, Xiangfang Li, Richard Wilkins, Pamela Obiomon, and Lijun Qian. Inverse quantum fourier transform inspired algorithm for unsupervised image segmentation. *arXiv preprint arXiv:2301.04705*, 2023. 2
- [4] Najd Alosaimi, Haikel Alhichri, Yakoub Bazi, Belgacem Ben Youssef, and Naif Alajlan. Self-supervised learning for remote sensing scene classification under the few shot scenario. *Scientific Reports*, 13(1):433, 2023. 2
- [5] Rasha Alshehhi and Prashanth Reddy Marpu. Hierarchical graph-based segmentation for extracting road networks from high-resolution satellite images. *ISPRS journal of photogrammetry and remote sensing*, 126:245–260, 2017. 2
- [6] Vishmi Fernando Anuradha Mahasinghe and Paduma Samarawickrama. Qubo formulations of three np problems. *Journal of Information and Optimization Sciences*, 42(7):1625–1648, 2021. 3
- [7] Federica Arrigoni, Willi Menapace, Marcel Seelbach Benkner, Elisa Ricci, and Vladislav Golyanik. Quantum motion segmentation. In *Computer Vision – ECCV 2022*, pages 506–523, Cham, 2022. Springer Nature Switzerland. 1
- [8] Mayowa Ayodele. Penalty weights in qubo formulations: Permutation problems. In *Evolutionary Computation in Combinatorial Optimization*, pages 159–174, Cham, 2022. Springer International Publishing. 2
- [9] Thorsten Beier, Thorben Kroeger, Jörg H. Kappes, Ullrich Köthe, and Fred A. Hamprecht. Cut, glue, & cut: A fast, approximate solver for multicut partitioning. In *2014 IEEE Conference on Computer Vision and Pattern Recognition*, pages 73–80, 2014. 2
- [10] Marcel Seelbach Benkner, Zorah Lähner, Vladislav Golyanik, Christof Wunderlich, Christian Theobalt, and Michael Moeller. Q-match: Iterative shape matching via quantum annealing. In *2021 IEEE/CVF International Conference on Computer Vision (ICCV)*, pages 7566–7576, 2021. 1
- [11] Harshil Bhatia, Edith Tretschk, Zorah Lähner, Marcel Benkner, Michael Möller, Christian Theobalt, and Vladislav Golyanik. Ccuantumm: Cycle-consistent quantum-hybrid matching of multiple shapes. In *IEEE Conference on Computer Vision and Pattern Recognition (CVPR)*, 2023. 1
- [12] Thomas Blaschke, Stefan Lang, Eric Lorup, Josef Strobl, and Peter Zeil. Object-oriented image processing in an integrated gis/remote sensing environment and perspectives for environmental applications. *Environmental information for planning, politics and the public*, 2:555–570, 2000. 2
- [13] Thomas Blaschke, Charles Burnett, and Anssi Pekkarinen. Image segmentation methods for object-based analysis and classification. *Remote sensing image analysis: Including the spatial domain*, pages 211–236, 2004. 2
- [14] Sergio Boixo, Vadim N. Smelyanskiy, Alireza Shabani, Sergei V. Isakov, Mark Dykman, Vasil S. Denchev, Mohammad H. Amin, Anatoly Yu Smirnov, Masoud Mohseni, and Hartmut Neven. Computational multiqubit tunnelling in programmable quantum annealers. *Nature Communications*, 7(1):10327, 2016. 3
- [15] Derrick Bonafilia, Beth Tellman, Tyler Anderson, and Erica Issenberg. Sen1floods11: A georeferenced dataset to train and test deep learning flood algorithms for sentinel-1. In *Proceedings of the IEEE/CVF Conference on Computer Vision and Pattern Recognition (CVPR) Workshops*, 2020. 2, 5
- [16] Kelly Boothby, Paul Bunyk, Jack Raymond, and Aidan Roy. Next-generation topology of d-wave quantum processors. *arXiv preprint arXiv:2003.00133*, 2020. 5
- [17] M. Born and V. Fock. Beweis des adiabatenatzes. *Zeitschrift für Physik*, 51(3):165–180, 1928. 3
- [18] Francesco Bova, Avi Goldfarb, and Roger G. Melko. Commercial applications of quantum computing. *EPJ Quantum Technology*, 8(1):2, 2021. 1
- [19] Ulrik Brandes and Thomas Erlebach, editors. *Network Analysis: Methodological Foundations*. Springer Berlin Heidelberg, 1 edition, 2005. 6
- [20] Jun Cai, William G Macready, and Aidan Roy. A practical heuristic for finding graph minors. *arXiv preprint arXiv:1406.2741*, 2014. 5, 8
- [21] Bo cai Gao. Ndwi—a normalized difference water index for remote sensing of vegetation liquid water from space. *Remote Sensing of Environment*, 58(3):257–266, 1996. 5
- [22] K Sante Camilus and VK Govindan. A review on graph based segmentation. *International Journal of Image, Graphics and Signal Processing*, 4(5):1, 2012. 2

- [23] Simona Caraiman and Vasile Manta. Image segmentation on a quantum computer. *Quantum Information Processing*, 14, 2015. 2
- [24] Vibhor Chauhan, Swati Negi, Dhyanendra Jain, Prashant Singh, Anil Kumar Sagar, and Anupam Kumar Sharma. Quantum computers: A review on how quantum computing can boom ai. In *2022 2nd International Conference on Advance Computing and Innovative Technologies in Engineering (ICACITE)*, pages 559–563, 2022. 1
- [25] Shuchao Chen, Han Yang, Jiawen Fu, Weijian Mei, Shuai Ren, Yifei Liu, Zhihua Zhu, Lizhi Liu, Haojiang Li, and Hongbo Chen. U-net plus: Deep semantic segmentation for esophagus and esophageal cancer in computed tomography images. *IEEE Access*, 7:82867–82877, 2019. 1
- [26] Heng-Da Cheng, X. H. Jiang, Ying Sun, and Jingli Wang. Color image segmentation: advances and prospects. *Pattern recognition*, 34(12):2259–2281, 2001. 2
- [27] D. Comaniciu and P. Meer. Robust analysis of feature spaces: color image segmentation. In *Proceedings of IEEE Computer Society Conference on Computer Vision and Pattern Recognition*, pages 750–755, 1997. 2
- [28] Sravan Danda, Aditya Challa, B. S. Daya Sagar, and Laurent Najman. Revisiting the isoperimetric graph partitioning problem. *IEEE Access*, 7:50636–50649, 2019. 2
- [29] Ilke Demir, Krzysztof Koperski, David Lindenbaum, Guan Pang, Jing Huang, Saikat Basu, Forest Hughes, Devis Tuia, and Ramesh Raskar. Deepglobe 2018: A challenge to parse the earth through satellite images. In *The IEEE Conference on Computer Vision and Pattern Recognition (CVPR) Workshops*, 2018. 2, 5
- [30] Balázs Dezso, Roberto Giachetta, István László, and István Fekete. Experimental study on graph-based image segmentation methods in the classification of satellite images. *EARSeL eProceedings*, 11(1):12–24, 2012. 2
- [31] Ping Fan, Ri-Gui Zhou, Wen Wen Hu, and NaiHuan Jing. Quantum image edge extraction based on laplacian operator and zero-cross method. *Quantum Information Processing*, 18(1):27, 2018. 1
- [32] Pedro F. Felzenszwalb and Daniel P. Huttenlocher. Efficient graph-based image segmentation. *International Journal of Computer Vision*, 59(2):167–181, 2004. 2
- [33] Pedro F Felzenszwalb and Daniel P Huttenlocher. Efficient graph-based image segmentation. *International journal of computer vision*, 59:167–181, 2004. 2
- [34] David B. Gillis and Jeffrey H. Bowles. Hyperspectral image segmentation using spatial-spectral graphs. In *Algorithms and Technologies for Multispectral, Hyperspectral, and Ultraspectral Imagery XVIII*, page 83901Q. International Society for Optics and Photonics, SPIE, 2012. 2
- [35] Fred Glover, Gary Kochenberger, and Yu Du. A tutorial on formulating and using qubo models. *arXiv preprint arXiv:1811.11538*, 2018. 3, 4
- [36] Fred Glover, Gary Kochenberger, and Yu Du. Applications and computational advances for solving the qubo model. In *The Quadratic Unconstrained Binary Optimization Problem: Theory, Algorithms, and Applications*, pages 39–56. Springer, 2022. 3
- [37] Enrique González-Arangüena, Conrado Miguel Manuel, and Mónica del Pozo. Values of games with weighted graphs. *European Journal of Operational Research*, 243(1): 248–257, 2015. 3
- [38] Stephen Gould, Tianshi Gao, and Daphne Koller. Region-based segmentation and object detection. In *Advances in Neural Information Processing Systems*. Curran Associates, Inc., 2009. 2
- [39] Edward Grant, Marcello Benedetti, Shuxiang Cao, Andrew Hallam, Joshua Lockhart, Vid Stojevic, Andrew G Green, and Simone Severini. Hierarchical quantum classifiers. *npj Quantum Information*, 4(1):65, 2018. 1
- [40] Kevin Iselborn, Marco Stricker, Takashi Miyamoto, Marlon Nuske, and Andreas Dengel. On the importance of feature representation for flood mapping using classical machine learning approaches. *arXiv preprint arXiv:2303.00691*, 2023. 5, 7
- [41] Jue Jiang, Yu-Chi Hu, Chia-Ju Liu, Darragh Halpenny, Matthew D. Hellmann, Joseph O. Deasy, Gig Mageras, and Harini Veeraraghavan. Multiple resolution residually connected feature streams for automatic lung tumor segmentation from ct images. *IEEE Transactions on Medical Imaging*, 38(1):134–144, 2019. 1
- [42] Anwesh Kabiraj, Debojyoti Pal, Debayan Ganguly, Kingshuk Chatterjee, and Sudipta Roy. Number plate recognition from enhanced super-resolution using generative adversarial network. *Multimedia Tools and Applications*, 82(9):13837–13853, 2023. 1
- [43] Kirill P. Kalinin and Natalia G. Berloff. Computational complexity continuum within ising formulation of np problems. *Communications Physics*, 5(1):20, 2022. 3
- [44] David R. Karger and Clifford Stein. A new approach to the minimum cut problem. *J. ACM*, 43(4):601–640, 1996. 3
- [45] Richard M. Karp. *Reducibility Among Combinatorial Problems*, pages 219–241. Springer Berlin Heidelberg, Berlin, Heidelberg, 2010. 3
- [46] Wonjik Kim, Asako Kanezaki, and Masayuki Tanaka. Unsupervised learning of image segmentation based on differentiable feature clustering. *IEEE Transactions on Image Processing*, 29:8055–8068, 2020. 2
- [47] Andrew D King and William Bernoudy. Performance benefits of increased qubit connectivity in quantum annealing 3-dimensional spin glasses. *arXiv preprint arXiv:2009.12479*, 2020. 6
- [48] Ioannis Kotaridis and Maria Lazaridou. Remote sensing image segmentation advances: A meta-analysis. *ISPRS Journal of Photogrammetry and Remote Sensing*, 173:309–322, 2021. 1, 2
- [49] Harashta Tatimma Larasati, Thi-Thu-Huong Le, and Howon Kim. Trends of quantum computing applications to computer vision. In *2022 International Conference on Platform Technology and Service (PlatCon)*, pages 7–12, 2022. 2
- [50] Andrew Lucas. Ising formulations of many np problems. *Frontiers in Physics*, 2:5, 2014. Edited by Jacob Biamonte, ISI Foundation, Italy. 3, 4
- [51] S. K. McFEETERS. The use of the normalized difference water index (ndwi) in the delineation of open water features.

- International Journal of Remote Sensing*, 17(7):1425–1432, 1996. 5
- [52] Catherine McGeoch and Pau Farré. The d-wave advantage system: An overview. *D-Wave Systems Inc., Burnaby, BC, Canada, Tech. Rep.*, 2020. 4, 5
- [53] Catherine McGeoch, Pau Farre, and William Bernoudy. D-wave hybrid solver service+ advantage: Technology update. *Tech. Rep.*, 2020. 5
- [54] Himanshu Mittal, Avinash Chandra Pandey, Mukesh Saraswat, Sumit Kumar, Raju Pal, and Garv Modwel. A comprehensive survey of image segmentation: clustering methods, performance parameters, and benchmark datasets. *Multimedia Tools and Applications*, 81(24):35001–35026, 2022. 2
- [55] Kumar Navulur. *Multispectral image analysis using the object-oriented paradigm*. CRC press, 2006. 2
- [56] Hartmut Neven, Vasil S Denchev, Geordie Rose, and William G Macready. Training a binary classifier with the quantum adiabatic algorithm. *arXiv preprint arXiv:0811.0416*, 2008. 1
- [57] Hartmut Neven, Geordie Rose, and William G Macready. Image recognition with an adiabatic quantum computer i. mapping to quadratic unconstrained binary optimization. *arXiv preprint arXiv:0804.4457*, 2008. 1
- [58] Harmut Neven, Vasil S Denchev, Marshall Drew-Brook, Jiayong Zhang, William G Macready, and Geordie Rose. Nips 2009 demonstration: Binary classification using hardware implementation of quantum annealing. *Quantum*, 4:1, 2009. 1
- [59] Andrew Ng, Michael Jordan, and Yair Weiss. On spectral clustering: Analysis and an algorithm. In *Advances in Neural Information Processing Systems*. MIT Press, 2001. 5
- [60] Soronzonbold Otgonbaatar and Mihai Datcu. Quantum annealing approach: Feature extraction and segmentation of synthetic aperture radar image. In *IGARSS 2020 - 2020 IEEE International Geoscience and Remote Sensing Symposium*, pages 3692–3695, 2020. 2
- [61] Nobuyuki Otsu. A threshold selection method from gray-level histograms. *IEEE transactions on systems, man, and cybernetics*, 9(1):62–66, 1979. 2
- [62] Shumao Pang, Chunlan Pang, Lei Zhao, Yangfan Chen, Zhihai Su, Yujia Zhou, Meiyang Huang, Wei Yang, Hai Lu, and Qianjin Feng. Spineparsenet: Spine parsing for volumetric mr image by a two-stage segmentation framework with semantic image representation. *IEEE Transactions on Medical Imaging*, 40(1):262–273, 2021. 1
- [63] S Prasad et al. Remotely sensed data characterization, classification, and accuracies. *CRC Press*, 1(6):7, 2015. 2
- [64] Timothe Presles, Cyrille Enderli, Gilles Burel, and El Housain Baghious. Synthetic aperture radar image segmentation with quantum annealing. *arXiv preprint arXiv:2305.17954*, 2023. 1, 2, 4, 8
- [65] O. Ronneberger, P.Fischer, and T. Brox. U-net: Convolutional networks for biomedical image segmentation. In *Medical Image Computing and Computer-Assisted Intervention (MICCAI)*, pages 234–241. Springer, 2015. (available on arXiv:1505.04597 [cs.CV]). 2
- [66] Janya Sainui and Paiboon Pattanasatean. Color classification based on pixel intensity values. In *2018 19th IEEE/ACIS International Conference on Software Engineering, Artificial Intelligence, Networking and Parallel/Distributed Computing (SNPD)*, pages 302–306, 2018. 2
- [67] M. Sankari and C. Meena. Enhanced Approaches to Rectify the Noise, Illumination and Shadow Artifacts. *International Journal of Information, Control and Computer Sciences*, 6,0 (10), 2018. 2
- [68] Mehmet Sezgin and Bülent Sankur. Survey over image thresholding techniques and quantitative performance evaluation. *Journal of Electronic Imaging*, 13(1):146 – 165, 2004. 2
- [69] Wei-Kuan Shih, Sun Wu, and Y.S. Kuo. Unifying maximum cut and minimum cut of a planar graph. *IEEE Transactions on Computers*, 39(5):694–697, 1990. 3
- [70] Irwin Sobel, Gary Feldman, et al. A 3x3 isotropic gradient operator for image processing. *Presentation at Stanford A.I. Project 1968*, pages 271–272, 1968. 2
- [71] Bhumika Solanki and Maya Ingle. Performance evaluation of thresholding techniques on modi script. In *2018 International Conference on Advanced Computation and Telecommunication (ICACAT)*, pages 1–6, 2018. 2
- [72] S. Sural, Gang Qian, and S. Pramanik. Segmentation and histogram generation using the hsv color space for image retrieval. In *Proceedings. International Conference on Image Processing*, pages II–II, 2002. 5
- [73] Lisa Tse, Peter Mountney, Paul Klein, and Simone Severini. Graph cut segmentation methods revisited with a quantum algorithm. *arXiv preprint arXiv:1812.03050*, 2018. 1, 2
- [74] Supreeth Mysore Venkatesh, Antonio Macaluso, and Matthias Klusch. Bilp-q: Quantum coalition structure generation. In *Proceedings of the 19th ACM International Conference on Computing Frontiers*, page 189–192, New York, NY, USA, 2022. Association for Computing Machinery. 4
- [75] Supreeth Mysore Venkatesh, Antonio Macaluso, and Matthias Klusch. Gcs-q: Quantum graph coalition structure generation. In *Computational Science – ICCS 2023*, pages 138–152, Cham, 2023. Springer Nature Switzerland. 4
- [76] Sara Vicente, Vladimir Kolmogorov, and Carsten Rother. Graph cut based image segmentation with connectivity priors. In *2008 IEEE Conference on Computer Vision and Pattern Recognition*, pages 1–8, 2008. 2
- [77] Yan Wang, Jian Cheng, Yixin Chen, Shuai Shao, Lanyun Zhu, Zhenzhou Wu, Tao Liu, and Haogang Zhu. FVP: Fourier visual prompting for source-free unsupervised domain adaptation of medical image segmentation. *IEEE Transactions on Medical Imaging*, pages 1–1, 2023. 2
- [78] Yiqun Xie, Zhili Li, Han Bao, Xiaowei Jia, Dongkuan Xu, Xun Zhou, and Sergii Skakun. Auto-cm: Unsupervised deep learning for satellite imagery composition and cloud masking using spatio-temporal dynamics. In *Proceedings of the Thirty-Seventh AAAI Conference on Artificial Intelligence and Thirty-Fifth Conference on Innovative Applications of Artificial Intelligence and Thirteenth Symposium on Educational Advances in Artificial Intelligence*. AAAI Press, 2023. 2

- [79] Pengao Xu, Zhenxing He, Tianhui Qiu, and Hongyang Ma. Quantum image processing algorithm using edge extraction based on kirsch operator. *Opt. Express*, 28(9):12508–12517, 2020. [1](#)
- [80] Tianyuan Yao, Chang Qu, Quan Liu, Ruining Deng, Yuanhan Tian, Jiachen Xu, Aadarsh Jha, Shunxing Bao, Mengyang Zhao, Agnes B. Fogo, Bennett A. Landman, Catie Chang, Haichun Yang, and Yuankai Huo. Compound figure separation of biomedical images with side loss. In *Deep Generative Models, and Data Augmentation, Labelling, and Imperfections*, pages 173–183, Cham, 2021. Springer International Publishing. [1](#)
- [81] Xi-Wei Yao, Hengyan Wang, Zeyang Liao, Ming-Cheng Chen, Jian Pan, Jun Li, Kechao Zhang, Xingcheng Lin, Zhehui Wang, Zhihuang Luo, Wenqiang Zheng, Jianzhong Li, Meisheng Zhao, Xinhua Peng, and Dieter Suter. Quantum image processing and its application to edge detection: Theory and experiment. *Phys. Rev. X*, 7:031041, 2017. [1](#)
- [82] Faliu Yi and Inkyu Moon. Image segmentation: A survey of graph-cut methods. In *2012 international conference on systems and informatics (ICSAI2012)*, pages 1936–1941. IEEE, 2012. [2](#)
- [83] Ying Yu, Chunping Wang, Qiang Fu, Renke Kou, Fuyu Huang, Boxiong Yang, Tingting Yang, and Mingliang Gao. Techniques and challenges of image segmentation: A review. *Electronics*, 12(5), 2023. [1](#)
- [84] Jan-Nico Zaech, Alexander Liniger, Martin Danelljan, Dengxin Dai, and Luc Van Gool. Adiabatic quantum computing for multi object tracking. In *2022 IEEE/CVF Conference on Computer Vision and Pattern Recognition (CVPR)*, pages 8801–8812, 2022. [1](#)
- [85] Xueliang Zhang, Xuezhi Feng, Pengfeng Xiao, Guangjun He, and Liujun Zhu. Segmentation quality evaluation using region-based precision and recall measures for remote sensing images. *ISPRS Journal of Photogrammetry and Remote Sensing*, 102:73–84, 2015. [1](#)